Horizontal Ice Velocity Estimation and Grounding Zone Detection in the Surroundings of Schirmacheroase, Antarctica, Using SAR Interferometry

By Robert Metzig[1], Reinhard Dietrich[1], Wilfried Korth[1], James Perlt[1], Rolf Hartmann[2] and Wolfgang Winzer[2]

Summary: Repeat-pass synthetic aperture radar (SAR) interferometry is utilized to estimate the ice velocity field and to locate the grounding line between grounded ice and floating ice shelf in the surroundings of the Schirmacheroase (71°S, 12°E). Because the interferometric phase is sensitive only to one component of the displacement vector ascending and descending passes are combined to derive the horizontal ice velocity field of the inland ice. By analysing this two-dimensional flow field the shape of the main ice stream in the vicinity of the Schirmacheroase is obtained. A migration of the grounding line of about 4.5 km is discovered where the main ice stream begins to float. This migration is very probably caused by ocean tides. To assess the accuracy of the interferometry results ground truth data are used.

Zusammenfassung: Die „Synthetic Aperture Radar" (SAR)-Interferometrie wird zur Bestimmung des Geschwindigkeitsfeldes von Eis und zur Lokalisierung der Aufsetzlinie zwischen gegrundetem Eis und schwimmendem Schelfeis in der Umgebung der Schirmacheroase (71°S, 12°O) angewandt. Da die interferometrische Phase nur Informationen über eine Komponente des Verschiebungsvektors beinhaltet, werden für den Bereich des Inlandeises aufsteigende und absteigende Orbits zur Ableitung des horizontalen Geschwindigkeitsfeldes kombiniert. Durch die Auswertung dieses zweidimensionalen Bewegungsfeldes können Ausdehnung und Verlauf des Haupteisstromes in der Nähe der Schirmacheroase bestimmt werden. Für den Übergangsbereich Inlandeis-Schelfeis des Haupteisstromes wird eine Migration der Aufsetzlinie von ungefähr 4.5 km nachgewiesen. Diese ist im wesentlichen eine Folge der Ozeangezeiten. Um die Genauigkeit der Interferometrieergebnisse zu bewerten, wird ein Vergleich mit Bodenkontrolldaten durchgeführt.

INTRODUCTION

Over 99 % of the land ice on Earth is stored in the ice sheets of Antarctica and Greenland (OERLEMANS 1993). Most of their volume is grounded and lies above sea level. Thus, a change of only a small fraction of this volume could affect the global sea level. Certain statements concerning the sign of its present contribution to changes in sea level require a more precise determination of the mass balance of polar ice sheets (BENTLEY & GIOVINETTO 1991, WARRICK et al. 1996). In this context the ice mass flux across the boundary between grounded and floating ice (i.e., the grounding line) should be considered rather then iceberg calving WARRICK et al. 1996). To calculate this mass flux, ice velocities and the grounding line position are needed beside other information. Repeat-pass SAR interferometry can be applied to determine surface velocity fields (JOUGHIN et al. 1996, JOUGHIN et al. 1998) as well as to detect the grounding line position (GOLDSTEIN et al. 1993, HARTL et al. 1994, RIGNOT 1996, DIETRICH et al. 1998a) including its migration due to glacier re-

cession or ocean tides (RIGNOT 1998a,b). However, a lack of available ground truth data restrict the possibilities to fully validate obtained results (JOUGHIN et al. 1998). In this paper, the accuracy and the reliability of interferometry results are investigated in the region of Schirmacheroase, Antarctica, using the extensive ground truth information available for this area.

First the working area and the available data are briefly described (Section 2). Section 3 focusses on the interferometric estimation of the horizontal ice velocity field for an inland ice area in the vicinity of Schirmacheroase. Especially the possibility of product improvement by means of corner reflectors is emphasized. To validate the interferometry results a comparison with ground truth data is performed. Finally, SAR interferometry is applied at different tidal heights to detect the grounding zone (Section 4).

WORKING AREA AND AVAILABLE DATA

At the edge of the Antarctic continent the ice-free Schirmacheroase is part of the boundary between the Nivlisen (ice shelf) and the inland ice area (Fig. 1). Since 1988, primarily ground based geodetic measurements have been carried out to determine glaciological parameters in the surroundings of the oasis. Several times three geodetic traverses were observed, providing coordinates and heights of points and profiles. The traverses cross the inland ice and the Nivlisen, resp. Coordinate changes between different epochs were used to calculate ice surface velocities. In addition to distance and direction measurements, since 1995 Global Positioning System (GPS) observations have been performed to obtain point coordinates and, finally, ice velocities for the both traverses south of the oasis (KORTH & DIETRICH 1996, KORTH et al. 1996). Summarizing the error budget for all epochs and for different ground based observation techniques, the total error of the ice surface velocity is smaller than 5%. Within the limits of this measurement accuracy there is no temporal variation in ice motion. Thus, this region is suited for the validation of interferometric velocity estimates.

In 1996, a few weeks before the SAR data acquisition, four corner reflectors were set up and observed by GPS (PERLT et al. 1996). The locations of the corner reflectors are marked as black triangles in Figure 1. Primarily, these reflectors serve as tie-points for the SAR analysis. The two northern reflectors are on

[1] Institut für Planetare Geodäsie, TU Dresden, D-01062 Dresden, Germany
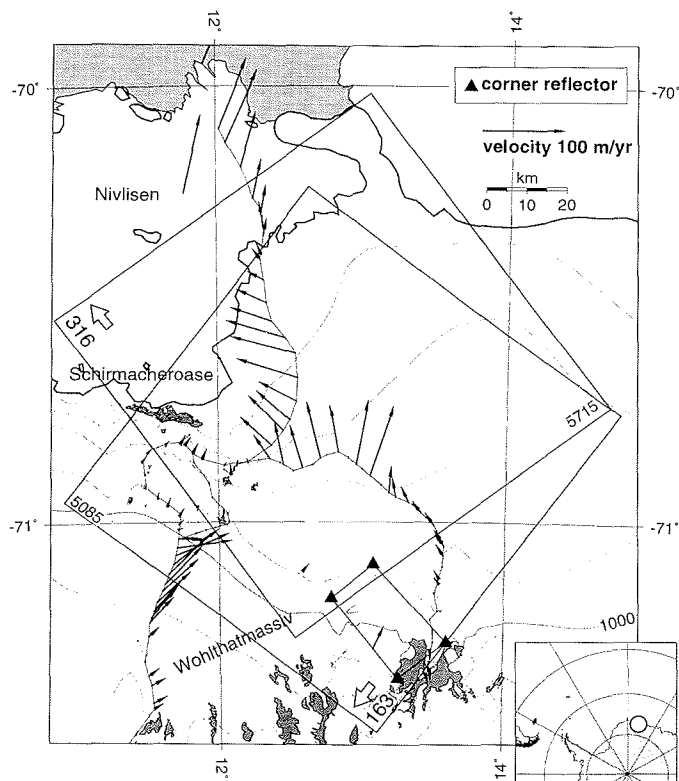[2] Jena-Optronik GmbH, Prüssingstraße 41, D-07745 Jena, Germany

Fig. 1: Map of the working area. Overlapping boxes denote regions covered by selected SAR images for ascending and descending passes of ERS-1&2 satellites. Black arrows indicate ice velocities from ground based measurements. The black line touching Schirmacheroase in the north represents the grounding line between floating ice shelf (e.g. the Nivlisen) and grounded inland ice.

Abb. 1: Karte des Arbeitsgebietes. Die überlappenden Boxen kennzeichnen Gebiete, die in den ausgewählten SAR-Szenen aufsteigender und absteigender Überflüge der ERS-1&2-Satelliten enthalten sind. Schwarze Pfeile zeigen Eisgeschwindigkeiten aus bodengebundenen Messungen. Die schwarze Linie, welche die Schirmacheroase nördlich berührt, stellt die Aufsetzlinie zwischen schwimmendem Schelfeis (z.B. das Nivlisen) und gegrundetem Inlandeis dar.

Fig. 2: Corner reflector on inland ice. The mountains in the background are part of the Wohlthatmassiv.

Abb. 2: Winkelreflektor auf dem Inlandeis. Die Berge im Hintergrund sind Teil des Wohlthatmassives.

ice whereas the two southern reflectors were built in ice-free areas. To determine the velocity vectors for the two reflectors on slightly moving ice (Fig. 2) the GPS observations were repeated in 1998. The coordinates for the reference corner of each reflector were determined within the International Terrestrial Reference Frame 94 (ITRF94) based on the Scientific Committee on Antarctic Research (SCAR) GPS campaigns (DIETRICH et al. 1998b). The achieved accuracy of the geometrical reflector corner is better than ± 5 cm for each epoch. For the two reflectors on ice the calculated velocities are 7.84 ± 0.05 m/yr and 2.27 ± 0.05 m/yr, resp. The direction of reflector motion is known with an accuracy of better than ± 2°. For the interferometric analysis presented in this paper a digital elevation model (DEM) is needed. Surface heights, determined by GPS, by trigonometric levelling and by airborne radio echo sounding (RES) in combination with kinematic GPS, resp., could be merged into a DEM of the working area with an accuracy of about ± 10...30 m (KORTH et al. 1997). Tide gauge records close to the oasis, existing for ten month 1991/92, two month 1995 and two month 1998, can be used to predict ocean tides for the Nivlisen (DIETRICH et al. 1995, KORTH 1998). This enables a better interpretation of the grounding line migration, revealed by SAR interfe-

rometry. Taking into consideration the inverse barometer effect the residual error of the model prediction is about ± 4 cm.

In 1996, during the ERS-1&2 tandem mission, several consecutive passes of ERS-1&2 capable for SAR interferometry were acquired covering the Nivlisen and the inland ice in the surroundings of Schirmacheroase. Full scene single look complex images (SLCI) are utilized for the interferometric analysis. The short interferometric baselines during the time of acquisition are suitable for studying motion phenomena. The image couples used to estimate the velocity field and to detect the grounding zone are listed in Table 1.

Epoch	Orbit	Track	Frame	B_n[m]	Pass
05.04.1996 07:18 UTC	ERS-1 24700				
		163	5085	66.8	desc.
06.04.1996 07:18 UTC	ERS-2 5027				
20.05.1996 23:58 UTC	ERS-1 25354				
		316	5715	7.8	asc.
21.05.1996 23:58 UTC	ERS-2 5681				

Tab. 1: SAR image couples used for the estimation of the horizontal velocity field and the detection of the grounding zone. B_n designates the component of the interferometric baseline perpendicular to the radar line of sight for the image center. asc. – ascending; desc. – descending.

Tab. 1: Für die Bestimmung des horizontalen Geschwindigkeitsfeldes und die Erkennung der Aufsetzzone genutzte SAR-Bildpaare. B_n bezeichnet die Komponente der interferometrischen Basis senkrecht zur Radarblickrichtung für die Bildmitte. asc. – aufsteigend, desc. – absteigend

Fig. 3: Flattened and topography free interferograms (motion-only) used for the horizontal ice velocity estimation. Top: frame 5085 track 163 (descending orbital passes ERS-1/24700 and ERS-2/5027; B_n = 66.8m). Bottom: frame 5715 track 316 (ascending orbital passes ERS-1/25354 and ERS-2/5681; B_n = 7.8 m; baseline estimation using four corner reflectors).

Abb. 3: Für die Bestimmung der horizontalen Eisgeschwindigkeit genutzte Interferogramme, die den Einfluss der interferometrischen Basis auf die interferometrische Phase nicht mehr enthalten („Bewegungsinterferogramme"). Oben: Frame 5085 Track 163 (Überflüge der absteigenden Orbits ERS-1/24700 und ERS-2/5027; B_n = 66.8 m). Unten: Frame 5715 Track 316 (Überflüge der aufsteigenden Orbits ERS-1/25354 und ERS-2/5681; B_n = 7.8 m; Schätzung der interferometrischen Basis unter Verwendung von vier Winkelreflektoren).

HORIZONTAL ICE VELOCITY FIELD ESTIMATION

The study is restricted to the two-dimensional case ignoring the vertical component of the velocity vector, since the area under investigation shows only slight surface slopes. Concerning the main ice stream the average surface slope does not exceed 1...2 %. Thus, the error of the horizontal velocity estimate due to neglected surface slope should be small. The interferometric estimation of the three-dimensional ice-flow is discussed in detail by JOUGHIN et al. (1998).

Because the interferometric phase is sensitive only to one component of the displacement vector ascending and descending passes are combined to derive the horizontal ice velocity field of the inland ice. On floating ice shelf this approach is more complicated because the interferometric phase is influenced by tidal motion. The interferograms presented in this paper were composed using descending orbits 24700 (ERS-1) and 5027 (ERS-2) as well as ascending orbits 25354 (ERS-1) and 5681 (ERS-2). To determine the horizontal velocity field the overlapping frames 5085 (descending track) and 5715 (ascending track) shown in Figure 1 were chosen. The combination of descending and ascending orbital passes acquired 1 $^1/_2$ months apart (Tab. 1) is meaningful if the ice flows at a constant rate during this time. Ground based measurements showing no temporal variation in ice motion support such an assumption for the area under investigation. Furthermore, if a cold-based ice stream is supposed, which is frozen to its bed, no short-term variation of the ice velocity should occur.

Before velocity estimates can be made the interferometric phase fractions of the reference ellipsoid and the topography above this reference ellipsoid caused by the orbital baseline must be removed. Baseline errors due to the orbit inaccuracy affect in particular the synthesized phase ϕ_e of the reference ellipsoid needed for flattening the interferogram (see Appendix). Orbit errors cause residual fringes approximately parallel to the along track direction. Using precise ERS orbit products for the orbit couple 25354 and 5681 the motion-only interferogram shows a fringe pattern, which leads to the assumtion of such orbit errors. To reduce velocity errors due to orbit inaccuracy the interferometric baseline is estimated using the four corner reflectors with known positions, heights and displacement rates. The positions of the corner reflectors can be seen in Figure 1. Because two corner reflectors are situated outside frame 5715 the adjacent frame is included in this computation step. The baseline estimation is carried out by fixing the vertical component B_z to the value calculated from precise ERS orbit products and by computing the horizontal component B_y depending on the along-track position. A similar approach was already used by ZEBKER et al. (1994). The normal component B_n of the estimated baseline for the image center is about 7.8 m instead of about 9.0 m if original precise ERS orbits are used.

To remove the effect of topography, synthetic topography-only interferograms are generated from an independent DEM. By differencing mixed motion topograpy interferograms with topography-only interferograms the phase fraction due to topogra-
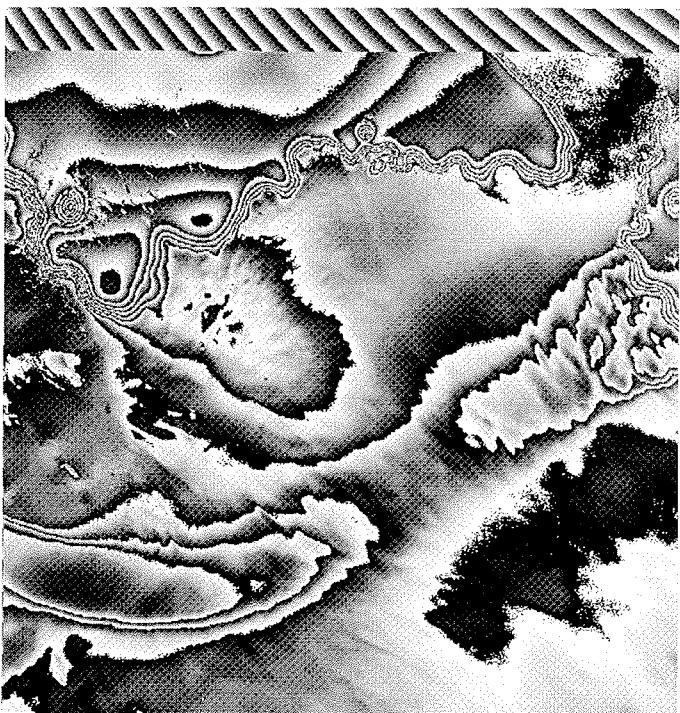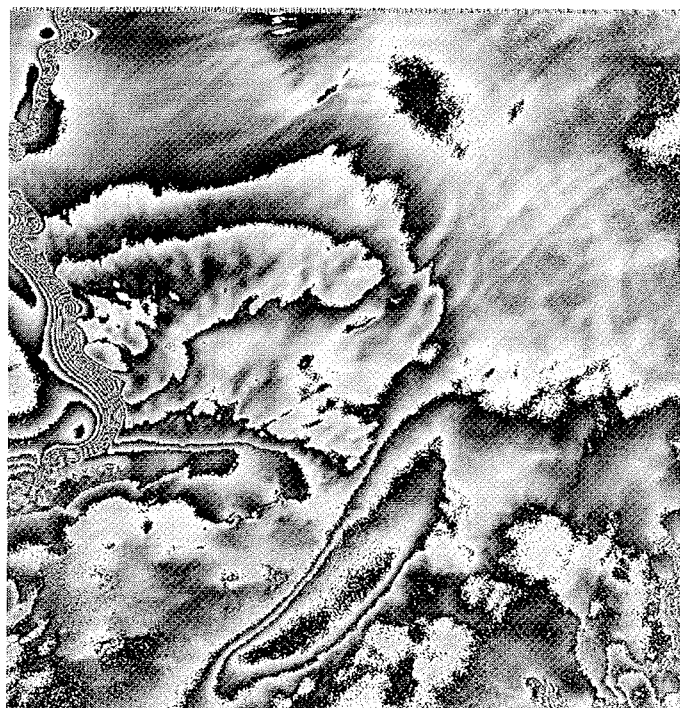
phy is cancelled. The resulting motion-only interferograms are shown in Figure 3. In our case there is no possibility to apply differential SAR interferometry for canceling the topography, since only ERS-1&2 tandem mission image couples are available. The velocity error caused by the inaccuracy of the used DEM is proportional to the baseline length and negligible for sufficient small baselines (GOLDSTEIN et al. 1993). For the ERS-1&2 tandem mission with a temporal baseline of 1 day a rough estimate for the velocity error $\sigma_{v,y,z}$ due to the DEM error s_z is 2.88 x 10^{-3} m^{-1} yr^{-1} B_n σ_z. Taking into consideration the accuracy of the DEM, a velocity error $\sigma_{v,y,z}$ of 0.2...0.7 m/yr for the ascending image couple and of 1.9...5.8 m/yr for the descending image couple, resp., is estimated (see Tab. 1).

In a next step the motion-only interferograms are unwrapped and referenced to a stationary earth fixed surface so that the sign of the unwrapped phase indicates the relative line of sight (slant range) displacement of the surface towards or off the SAR sensor. To derive ice velocities a geocoding of the image information of each unwrapped interferogram into ellipsoidal coordinates of the Geodetic Reference System 1980 (GRS80) is performed. The effect of terrain distortion due to the SAR System is removed by using the DEM. The corner reflectors serve as tie-points for the precise image co-registration of ascending and descending track. If a negligible surface slope is assumed the horizontal ice velocity field can be derived from the ascending and descendig track alone. No additional DEM derived slope information are needed.

Figure 4 shows the horizontal velocity field of the grounded ice sheet in the surroundings of the Schirmacheroase for the over-

lapping area of frame 5715 (track 316) and frame 5085 (track 163). Inside white masked areas phase unwrapping does not work. White arrows indicate the flow direction. The magnitude of ice velocity is gray scaled. If one looks at the velocity field a region is clearly visible in which the ice flows much faster than in the regions on either side. This faster moving region can be assigned to an active ice stream showing surface velocities up to 100 m/yr. There is no evidence of a second branch which has its source in the adjoining eastern lednik Éntuziastov supposed in HERMICHEN (1995). The wavy north-west edge of the velocity field denotes approximately the grounding line position where the ice begins to float. To access the accuracy of the results independent estimates of the ice velocity are used. Figure 5 shows the residuals between the ground truth and the interferometric velocity vectors. Concerning the magnitude of velocity the agreement is within few meters per year (Tab. 2). It should be noticed that the interferometric velocity values in meters per year base on surface displacements during consecutive passes of ERS-1&2 one day apart. That means, the combined analysis of interferometric velocity estimates of ascending and descending orbital passes is suited to derive surface displacements within the centimeter level. The remaining differences are presumably caused by errors of the used DEM to remove topography as discussed before and possible residual orbit errors of the descending track.
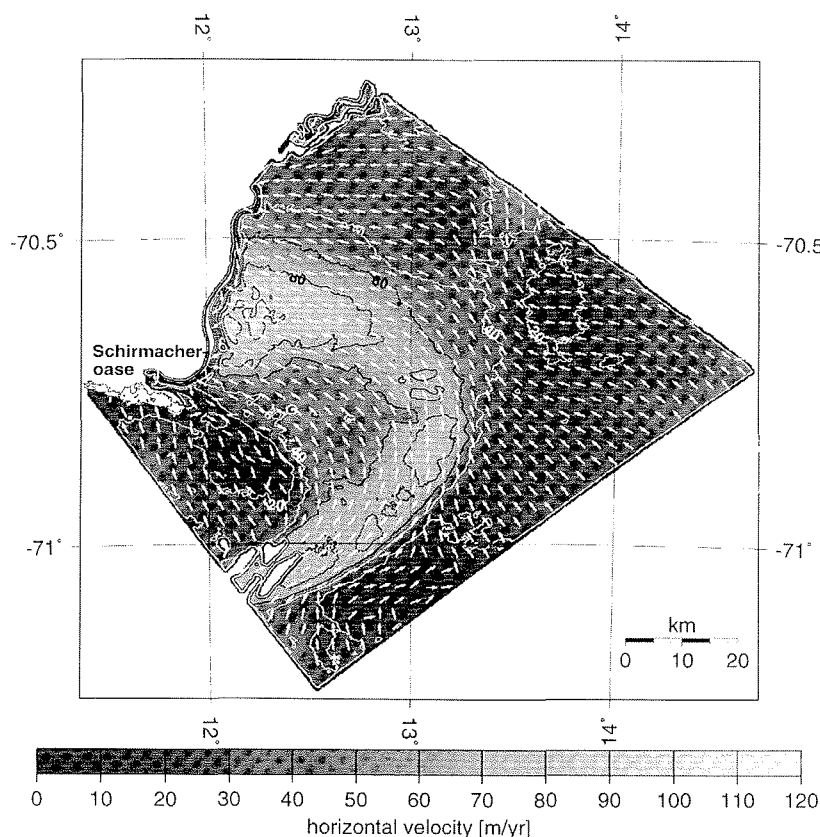

Fig. 4: Horizontal ice velocity field in the surroundings of the Schirmacheroase based on the interferometric analysis and combination of ascending and descending orbital passes of ERS-1&2. White arrows indicate the flow direction. The magnitude of ice velocity is gray scaled.

Abb. 4: Horizontales Eisgeschwindigkeitsfeld der Umgebung der Schirmacheroase, das auf der interferometrischen Auswertung und Kombination aufsteigender und absteigender ERS-1&2-Überflüge basiert. Weiße Pfeile kennzeichnen die Fließrichtung. Der Betrag der Eisgeschwindigkeit ist grau skaliert.

Fig. 5: Polar plot of residuals between interferometric displacement vectors and ground based displacement vectors (temporal baseline of one day). The ground based displacement vectors were computed from GPS observations in 1995 and 1998.

Abb. 5: Polardiagramm der Residuen zwischen interferometrisch abgeleiteten Verschiebungsvektoren und bodengebunden bestimmten Verschiebungsvektoren (zeitliche Basis von einem Tag). Die bodengebunden bestimmten Verschiebungsvektoren basieren auf GPS-Beobachtungen von 1995 und 1998.

Signal	v_{gt} [m/yr]	$v_{1/2}$ [m/yr]	$v_{gt} - v_{1/2}$ [m/yr]
U9	17.15	25.70	-8.55
U10	20.90	20.99	-0.09
U11	29.86	28.62	1.24
U13	80.84	83.81	-2.97
U14	58.03	56.93	1.10
U15	48.16	51.36	-3.20
U16	54.34	57.34	-3.00
U19	2.28	4.71	-2.43

Tab. 2: Comparison of magnitude v of ground based velocity vectors and interferometric velocity vectors. The interferometric velocity values in m/yr base on surface displacements during consecutive passe of ERS-1&2 (temporal baseline of one day). gt – ground truth; 1/2 – ERS-1&2.

Tab. 2: Vergleich des Betrages v bodengebunden bestimmter Geschwindigkeitsvektoren und interferometrisch abgeleiteter Geschwindigkeitsvektoren. Die interferometrisch ermittelten Geschwindigkeitswerte in m/a (m/yr) basieren auf Verschiebungen der Oberfläche während aufeinanderfolgender Überflüge von ERS-1&2 (zeitliche Basis von einem Tag). gt – Bodenkontrollwerte; 1/2 – ERS-1&2.

GROUNDING ZONE DETECTION

Caused by ocean tides and depending on surface and basal slope the grounding line migrates back and forth with time within a grounding zone (RIGNOT 1998b). The short-term grounding line migration due to ocean tides is investigated in detail within the ice stream.

The tidal flexing of the transition zone between grounded and nearly free floating ice shelf during different epochs can be used to detect the hinge line by means of SAR interferometry. The hinge line which indicates the limit of tidal flexing may not necessarily coincide with the true grounding line (SMITH 1991, RIGNOT 1996), but is used as the interferometric grounding line. Usually a quadruple difference interferometry technique (RIGNOT 1996, 1998a) is applied to remove the phase fraction due to steady ice creep flow to obtain tide-only interferograms. Since only single ERS-1&2 tandem couples are available for the working area (Tab. 1) this technique can not be utilized. Thus, the single geocoded motion-only interferograms of the descending track 163 (Fig. 6, top) and the ascending track 316 (Fig. 6, bottom) are compared. It is assumed that the clearly visible fringe belt with a significantly higher fringe frequency than in the remaining area of the respective motion-only interferogram is mainly caused by tidal flexing. The southern and the eastern edge of the fringe belt, resp., indicates the rough position of the grounding line. In Figure 6, top and bottom, the approximate intersection points of the ice stream center line with the grounding line are marked as white crosses. H and L denote the intersection points of the motion-only interferograms of the descending track 163 (Fig. 6, top) and of the ascending track 316 (Fig. 6, bottom). The distance between H and L is about 4.5 km. Taking into consideration the predicted ocean tides based on tide gauge records close to Schirmacheroase (Fig. 7) we attribute the grounding line position of Figure 6, top, to a sea level close to high tide and the grounding line position of Figure 6, bottom, to a sea level close to low tide. That means H and L represent the rough edges of the grounding zone for high and low tide concerning the ice stream center line.

The grounding line migration of about 4.5 km coincides with a predicted tidal height difference of less than 1.5 m and a surface slope of about 1 % inland. Applying a simple mathematical relation given in (RIGNOT 1998b) a subglacial topography can be expected, which deepens inland. In doing so it is assumed that no short-term (1 1/2 months) variations in ice thickness occur. Single RES measurements within the ice stream close to the grounding zone (DAMM et al. 1998) show a subglacial topography, which deepens inland too. However, the RES data themselves are too sparsely to make final statements. It can not be excluded that sedimentation within the grounding zone (see e.g. ALLEY et al. 1989) causes the assumed basal slope.

The obtained results, in particular the remarkable large short-term migration of the grounding line, confirm the fact that investigations of long-term changes for instance in ice thickness within ice streams or outlet glaciers requires the knowledge of the tidal-induced grounding line migration for each epoch.
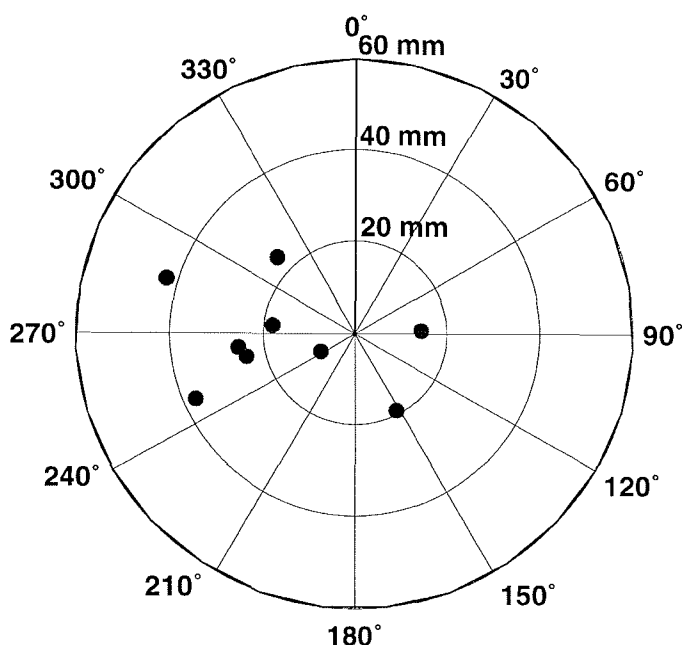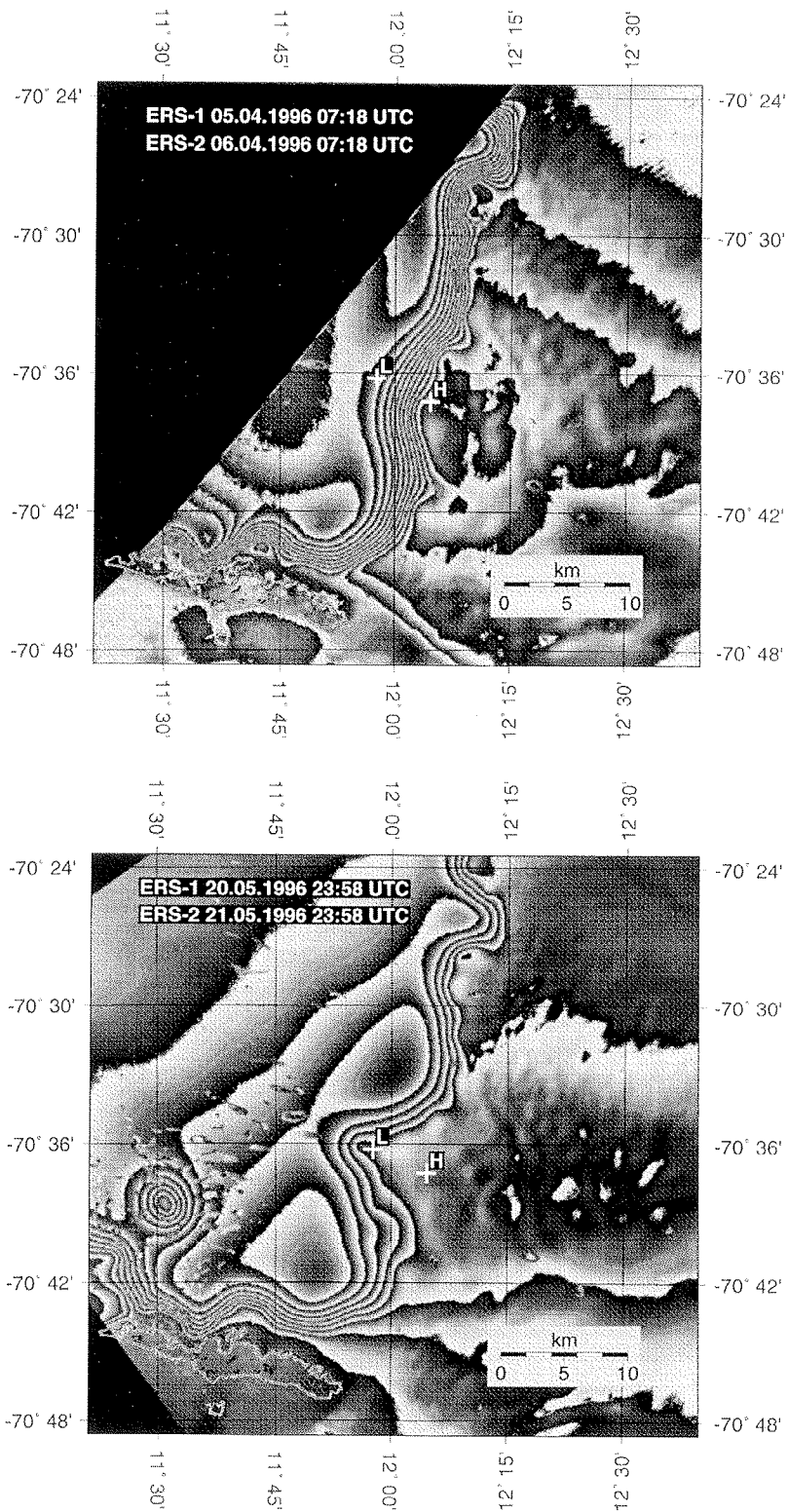
Fig. 6: Geocoded motion-only interferograms covering the same region of the ice stream north-east of Schirmacheroase used to detect the grounding zone. The outline of Schirmacheroase is visible in the lower left corner of the images. Top: descending orbital passes ERS-1/24700 and ERS-2/5027. Bottom: ascending orbital passes ERS-1/25354 and ERS-2/5681.

Abb. 6: Zur Erkennung der Aufsetzzone genutzte geokodierte „Bewegungsinterferogramme", die dasselbe Gebiet des Eisstromes nordöstlich der Schirmacheroase beinhalten. Die Kontur der Schirmacheroase ist in der unteren linken Bildecke sichtbar. Oben: Überflüge der absteigenden Orbits ERS-1/24700 und ERS-2/5027; Unten: Überflüge der aufsteigenden Orbits ERS-1/25354 und ERS-2/5681.
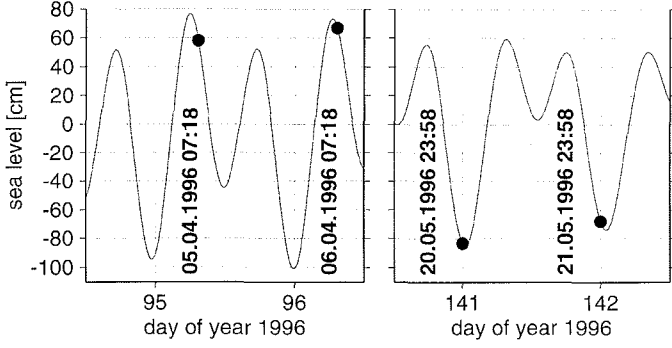
Fig. 7: Predicted sea level using tide gauge records close to Schirmacheroase (without barometric corrections). Black points indicate sea level values coincide with recording time of the used orbit couples. Left: descending orbital passes ERS-1/24700 and ERS-2/5027. Right: ascending orbital passes ERS-1/25354 and ERS-2/5681.

Abb. 7: Aus Pegelaufzeichnungen nahe der Schirmacheroase prädizierter Meeresspiegel (ohne barometrische Korrektionen). Schwarze Punkte kennzeichnen Meeresspiegelwerte, die mit der Aufzeichnungszeit der genutzten Orbitpaare übereinstimmen. Links: Überflüge der absteigenden Orbits ERS-1/24700 und ERS-2/5027; Rechts: Überflüge der aufsteigenden Orbits ERS-1/25354 und ERS-2/5681.

CONCLUSIONS

This study shows that SAR interferometry can be applied to detect the shape of ice streams even in featureless inland ice areas. The shape detection bases on the interferometric ice velocity field. Ascending and descending passes were combined to estimate the horizontal velocity field in the vicinity of Schirmacheroase. The comparison with ground truth data demonstrates the capability of SAR interferometry to provide surface displacements with an accuracy in the centimeter level.

The interferometric analysis revealed an extreme wide grounding zone within the ice stream close to the center line. The large grounding line migration coincide with a predicted tidal height difference of less than 1.5 m. With regard to the surface slope a behaviour like that requires theoretically a subglacial topography, which deepens inland. Concerning investigations of long-term changes for instance in ice thickness within ice streams or outlet glaciers there is a need to consider the tidal-induced changes of the grounding line for each epoch to obtain reliable results.

APPENDIX

Velocity Error Due to Orbit Inaccuracy

The making of an motion-only interferogram requires the removal of the interferometric phase fractions of the reference ellipsoid and the topography above this reference ellipsoid. Baseline errors due to the orbit inaccuracy affect in particular the synthesized phase ϕ_e of the reference ellipsoid needed for flattening the interferogram.

Since the velocity of any point can only be determined relatively to a point of known velocity the change of ϕ_e from slant range r_i to slant range r_j is considered for a fixed along-track position. Starting with

$$\phi_e = \tag{A.1}$$

$$-\frac{4\pi}{\lambda}\left[\sin\left(\theta_0 + \delta\theta_e\right)B_y - \cos\left(\theta_0 + \delta\theta_e\right)B_z + \frac{B^2}{2r}\right]$$

the change of ϕ_e from r_i to r_j is given by

$$\Delta\phi_{e,ij} = \tag{A.2}$$

$$-\frac{4\pi}{\lambda}\left[\sin\left(\theta_0 + \delta\theta_{e,j}\right) - \sin\left(\theta_0 + \delta\theta_{e,i}\right)\right]B_y$$

$$+\frac{4\pi}{\lambda}\left[\cos\left(\theta_0 + \delta\theta_{e,j}\right) - \cos\left(\theta_0 + \delta\theta_{e,i}\right)\right]B_z$$

$$-\frac{4\pi}{\lambda}\left[\frac{B^2}{2}\left(\frac{1}{r_j} - \frac{1}{r_i}\right)\right].$$

An expression containing the horizontal and vertical component of the baseline, B_y and B_z, resp., is chosen, since the orbit accuracy is different for the across track and the radial component of the orbit vector. B indicates the baseline length and $\delta\Theta_e$ is the angle between the reference-look direction and the intersection point of the slant range arc of radius r with the reference ellipsoid. A convenient choise is to let the nominal center-look angle Θ_0 define the reference-look direction (JOUGHIN et al. 1996). The SAR wavelength is denoted as λ. Neglecting small non-linear terms, the variance of $\Delta\phi_{e,ij}$ is

$$\sigma^2_{\Delta\phi_{e,ij},B} = \left(\frac{4\pi}{\lambda}\right)^2 \times \tag{A.3}$$

$$\left[\left(\left[\sin\left(\theta_0 + \delta\theta_{e,j}\right) - \sin\left(\theta_0 + \delta\theta_{e,i}\right)\right]\sqrt{2}\,\sigma_{S_y}\right)^2\right.$$

$$\left.+ \left(\left[\cos\left(\theta_0 + \delta\theta_{e,j}\right) - \cos\left(\theta_0 + \delta\theta_{e,i}\right)\right]\sqrt{2}\,\sigma_{S_z}\right)^2\right],$$

where $\sqrt{2}\sigma_{S_y} = \sigma_{B_y}$ and $\sqrt{2}\sigma_{S_z} = s_{B_z}$ assuming uncorrelated orbit error. σ_{S_y} and σ_{S_z} denote the accuracy of the respective orbit vector in across track and radial direction. For the precise ERS orbit products the respective values are about 30...100 cm across track (GEUDTNER 1995) and about 5 cm (SCHARROO & VISSER 1998) radial. If the vertical component of the ice velocity is neglected (a reasonable assumption for areas of slight surface slope) the variance of the relative velocity at r_j in relation to r_i due to the orbit inaccuracy can be expressed as

$$\sigma^2_{\Delta v_{y,ij},B} = \frac{2}{(\Delta t \sin\eta_j)^2} \times \tag{A.4}$$

$$\left[\left(\left[\sin\left(\theta_0 + \delta\theta_{e,j}\right) - \sin\left(\theta_0 + \delta\theta_{e,i}\right)\right]\sigma_{S_y}\right)^2\right.$$

$$\left.+ \left(\left[\cos\left(\theta_0 + \delta\theta_{e,j}\right) - \cos\left(\theta_0 + \delta\theta_{e,i}\right)\right]\sigma_{S_z}\right)^2\right]$$

η is the local incidence angle and Δt the temporal baseline of the interferogram. For the ERS-1&2 tandem mission Δt is one day for consecutive satellite passes covering the same track. In the worst case, that means an across track orbit error of 100 cm, a maximum phase error of about 5.2 x 2π for a 100 km wide

interferogram from near to far range or vice versa is possible. The possible 5 cm inaccuracy in radial direction do not change this value significantly. The phase error of 5.2 fringes corresponds to a velocity error of about 159 m/yr, concerning SAR data acquired one day apart. A similar error estimation is given by JOUGHIN et al. (1996). Assuming a perfect known across track component of the respective orbit vector an error of 5 cm in radial direction causes only a maximum phase error of about 0.1 x 2π from near to far range or vice versa corresponding to a velocity error of less than 3 m/yr.

ACKNOWLEDGMENT

References

Alley, R.B., Blankenship, D., Rooney, S.T. & Bentley, C.R. (1989): Sedimentation beneath ice shelves – the view from Ice Stream B.- Mar. Geol. 85: 101-120.

Bentley, C.R. & Giovinetto, M.B. (1991): Mass balance of Antarctica and and sea level change.- In: G. WELLER, C.L. WILSON & B.A.B. SEVERIN (eds.), Proceedings of the International Conference on the Role of the Polar Regions in Global Change. Univ. of Alaska, Fairbanks, 481-488.

Damm, V., Reitmayr, G., Korth, W., Dietrich, R. & Perlt, J. (1998): Ice thickness and subice morphology in central Queen Maud Land/East Antarctica deduced by radio echo soundings (RES).- Proceed. 7th Internat. Conf. Ground-Penetrating Radar. Univ. of Kansas, Lawrence, 27-30.

Dietrich, R., Liebsch, G., Dittfeld, H.J. & Noack, G. (1995): Ocean tide and attempt of Earth tide recordings at Schirmacher Oasis / Dronning Maud Land (Antarctica).- Proceed. 12th Internat. Sympos. Earth Tides, Sci. Press, Beijing, New York.

Dietrich, R., Dach, R., Korth, W., Metzig, R., Perlt, J., Hartmann, R. & Winzer, W. (1998a): Ice – Ocean – Solid Earth Interactions in Dronning Maud Land / Antarctica: A geodetic approach to solve open questions.- In: R. FORSBERG, M. FEISSL & R. DIETRICH (eds.), Geodesy on the move: Gravity, geoid, geodynamics, and Antarctica. Proc. IAG Sci. Assembly, Rio de Janeiro, Sept. 3-9, 1997, Springer Series: IAG Symposia, Vol. 119: 504-509, Springer, Heidelberg.

Dietrich, R., Dach, R., Perlt, J., Schenke, H. W., Schöne, T., Pohl, M., Soltau, G., Engelhardt, G., Mikolaiski, H. W., Seeber, G., Menge, F., Niemeier, W., Salbach, H., Lindner, K., Kutterer, H. & Mayer, M.(1998b): The SCAR GPS campaigns: Accurate geodetic reference in Antarctica.- In: R. FORSBERG, M. FEISSL & R. DIETRICH (eds.), Geodesy on the move: Gravity, geoid, geodynamics, and Antarctica. Proc. IAG Scientific Assembly, Rio de Janeiro, Sept. 3-9, 1997, Springer Series: IAG Symposia, Vol. 119: 474-479, Springer, Heidelberg.

Geudtner, D. (1995): Die interferometrische Verarbeitung von SAR-Daten des ERS-1.- DLR-Forschungsbericht 95-28. Deutsche Forschungsanstalt für Luft- und Raumfahrt Köln.

Goldstein, R.M., Engelhardt, H., Kamb, B. & Frolich, R.M. (1993): Satellite radar interferometry for monitoring ice sheet motion: Application to an Antarctic Ice Stream.- Science 262: 1525-1530.

Hartl, P., Thiel, K.-H., Wu, X., Doake, C.S.M. & Sievers, J. (1994): Application of SAR interferometry with ERS-1 in the Antarctic.- Earth Observation Quarterly 43: 1-4.

Hermichen, W.D. (1995): The continental ice cover in the surroundings of the Schirmacher Oasis.- In: P. BORMANN & D.FRITZSCHE (eds.), The Schirmacher Oasis, Queen Maud Land, East Antarctica, and its surroundings.- Justus Perthes Verlag, Gotha.

Joughin, I., Kwok, R. & Fahnestock, M. (1996): Estimation of ice-sheet motion using satellite radar interferometry: method and error analysis with application to Humboldt Glacier, Greenland.- J. Glaciol. 42: 564-575.

Joughin, I.R., Kwok, R. & Fahnestock, M.A. (1998): Interferometric estimation of three-dimensional ice-flow using ascending and descending passes.- IEEE Transactions Geosci. and Remote Sensing 36: 25-37.

Korth, W. & Dietrich, R. (1996): Ergebnisse geodätischer Arbeiten im Gebiet der Schirmacheroase / Antarktika 1988-1993.- Deutsche Geodätische Kommission, Reihe B, Heft 301, München.

Korth, W., Perlt, J., Dach, R. & Dietrich, R. (1996): Repeated observations of ice surface heights near Schirmacher Oasis for ice mass balance studies.- In: R. DIETRICH (ed.), The Geodetic Antarctic Project GAP95 – German contributions to the SCAR 95 Epoch Campaign.- Deutsche Geodätische Kommission, Reihe B, Heft 304, München.

Korth, W., Dietrich, R., Reitmayr, G. & Damm, V. (1997): Regional geoid improvement based on surface gravity data.- In: R. FORSBERG, M. FEISSL & R. DIETRICH (eds.), Geodesy on the move: Gravity, geoid, geodynamics, and Antarctica. Proc. of the IAG Scientific Assembly, Rio de Janeiro, Sept. 3-9, 1997, Springer Series: IAG Symposia, Vol. 119: 523-528, Springer, Heidelberg.

Korth, W. (1998): Bestimmung von Oberflächengeometrie, Punktbewegungen und Geoid in einer Region der Antarktis.- Deutsche Geodätische Kommission, Reihe C, Heft 505, München.

Oerlemans, J. (1993): Possible changes in the mass balance of the Greenland and Antarctic ice sheets and their effects on sea level.- In: R.A. WARRICK, E.M. BARROW & T.M.L. WIGLEY, (eds.), Climate and sea level change: Observations, projections and implications, Cambridge University Press.

Perlt, J., Korth, W., Dach, R. & Dietrich, R. (1996): Geodetic fieldwork in Dronning Maud Land within the framework of the GeoMaud Expedition 1995/96.- In: R. DIETRICH (ed.), The Geodetic Antarctic Projekt GAP 95 - German contributions to the SCAR 95 Epoch campaign.- Deutsche Geodätische Kommission, Reihe B, Heft 304, 143-146, München.

Rignot, E. (1996): Tidal motion, ice velocity and melt rate of Petermann Gletscher, Greenland, measured from radar interferometry.- J. Glaciol. 42: 476-485.

Rignot, E. (1998a): Hinge-line migration of Petermann Gletscher, north Greenland, detected using satellite-radar interferometry.- J. Glaciol. 44: 469-476.

Rignot, E. (1998b): Fast Recession of a West Antarctic Glacier.- Science 281: 549-551.

Scharroo, R. & Visser, P. (1998): Precise orbit determination and gravity field improvement for ERS satellites.- J. Geophys. Res. 103(C4): 8113-8127.

Smith, A.M. (1991): The use of tiltmeters to study the dynamics of Antarctic ice-shelf grounding lines.- J. Glaciol. 37: 51-58.

Warrick, R.A., Le Provost, C., Meier, M.F., Oerlemans, J. & Woodworth, P.L. (1996): Changes in sea level.- In: J.T. HOUGHTON, L.G. MEIRA FILHO, B.A. CALLANDER, N. HARRIS, A. KATTENBERG & K. MASKELL (eds.), Climate change 1995.- Cambridge University Press, Cambridge.

Zebker, H.A., Werner, C.L., Rosen, P.A., & Hensley, S. (1994): Accuracy of topographic maps derived from ERS-1 interferometric radar.- IEEE Trans. Geosci. and Remote Sensing 42: 823-836.